Please cite this article in press as: Gupta et al., Identification of *KLHL41* Mutations Implicates BTB-Kelch-Mediated Ubiquitination as an Alternate Pathway to..., The American Journal of Human Genetics (2013), http://dx.doi.org/10.1016/j.ajhg.2013.10.020

Table1. Clinical Manifestations in Affected Individuals Harboring *KLHL41* Mutations

Proband ID	cDNA Change	Amino Acid Change	Clinical Category	Sex	Nationality	Pregnancy and Delivery	Alive at Age/Mobility/ Age at Death	Associated Features
203-1	c.103T>C c.(?_-77)_(*602_?)del	p.Cys35Arg Heterozygous p.0? Heterozygous	Intermediate	F	Vietnamese	Normal	16 yrs, uses wheelchair (ambulant 24–36 mo)	Ventilated 24 hr from 5 yrs. High-arched palate, dysarthria Scoliosis
832-1	c.459delinsACTC	p.Ser153_Ala154insLeu Homozygous	Other forms (grade of severity: mild)	M	Russian	No data	12 yrs, ambulant	Distal weakness > proximal distal contractures
D10-236	c.581_583delAAG c.1238C>T	p.Glu194del Heterozygous p.Ser413Leu Heterozygous	Typical form	M	Chinese	Normal - h 40	5 yrs, ambulant	VSD, finger contractures, focal renal echogenicity
D12-203	c.1748_1755del AAGGAAAT,	p.Lys583Thrfs*7 Homozygous	Fetal akinesia sequence	M	Persian	Polyhydramnios, breech presentation, emergency Cesarean section - h 31+2	Died at 3 mo (active support discontinued)	Arthrogryposis, macrocephaly, hypospadias No antigravity movements at birth
12DG1177	c.641delA	p.Asn214Thrfs*14 Homozygous	Severe form Fetal akinesia sequence	M	Saudi Arabian	Fetal movements weak, breech presentation	Died during 1st day of life	Dislocation of hips and knees, cleft palate, micrognathia, narrow chest

mutations showed a segregation pattern compatible with a recessive mode of inheritance in all families (Figure S1). Severe phenotypes associated with genetic null mutations and intermediate or typical congenital forms with mutations that should results in presence of residual protein, suggests a phenotype-genotype correlation in individuals affected with *KLHL41* mutations.

KLHL41 belongs to the family of BTB-Kelch domain-containing proteins.[17–20] Mutations in two other members of this family, *KBTBD13* (MIM 613727), and most recently *KLHL40* (MIM 615430), have been associated with a clinically distinct form of congenital myopathy exhibiting nemaline bodies, as well as multiminicores and severe NM, respectively.[12,13] To evaluate the impacts of the *KLHL41* mutations on the protein structure, we mapped them onto the crystal structures of the BTB-BACK domain of human KLHL11 in complex with human CUL3, a subunit of E3 ubiquitin ligases, (PDB code 4AP2)[21] and the Kelch domain of rat KLHL41 (PDB code 2WOZ),[22] analogous to those domains of human KLHL41. The Cys35 side chain is involved in a hydrophobic core of the BTB domain, which makes van der Waals contacts with Phe54 of Cul3 (Figure 1B). The p.Cys35Arg substitution present in affected individual 203-1 would likely destabilize the hydrophobic core and thereby impair the interaction with Cul3. This was supported by the FoldX result, in which free energy change upon the p.Cys35Arg substitution was predicted to be over 4 kcal/mol, which can be interpreted as considerable destabilization of a protein structure (Figure 1D; Figure S3).[23] In proband 832-1, a Leu residue is inserted between the amino acid positions 153 and 154 in the center of a helix, in which several residues are involved in a hydrophobic core of the BACK domain (Figure 1B). This amino acid insertion is likely to destabilize the BACK domain fold. In proband D10-236, the p.Ser413Leu substitution was mapped to a loop region, which is located near the substrate-binding region of the Kelch repeat 2 (Figure 1C; Figure S1B). A FoldX calculation predicted that the p.Ser413Leu substitution would have minimal effect on stability of the Kelch domain (Figure 1D). The effect of Glu194 deletion at the N-terminal end of an α helix can be compensated by the presence of Glu193 located in the loop (Figure 1B). Nonetheless, it cannot be excluded that the p.Ser413Leu and p.Glu194del changes alter the protein solubility or aggregate tendency and/or impair substrate binding. The conserved nature of the mutated KLHL41 domains, as well as the potential role of the mutations in disrupting those structural domains, supports the likely pathogenicity of these mutations.

The localization of KLHL41 in skeletal muscles was investigated by immunofluorescence of mouse FDB cultured myofibers and human skeletal muscle cryosections. Immunofluorescence with two different antibodies against N-terminal (Sigma, AV38732) and C-terminal parts of human KLHL41 (Abcam, ab66605) was performed, and z stacks were acquired by confocal microscopy as described

Please cite this article in press as: Gupta et al., Identification of *KLHL41* Mutations Implicates BTB-Kelch-Mediated Ubiquitination as an Alternate Pathway to..., The American Journal of Human Genetics (2013), http://dx.doi.org/10.1016/j.ajhg.2013.10.020

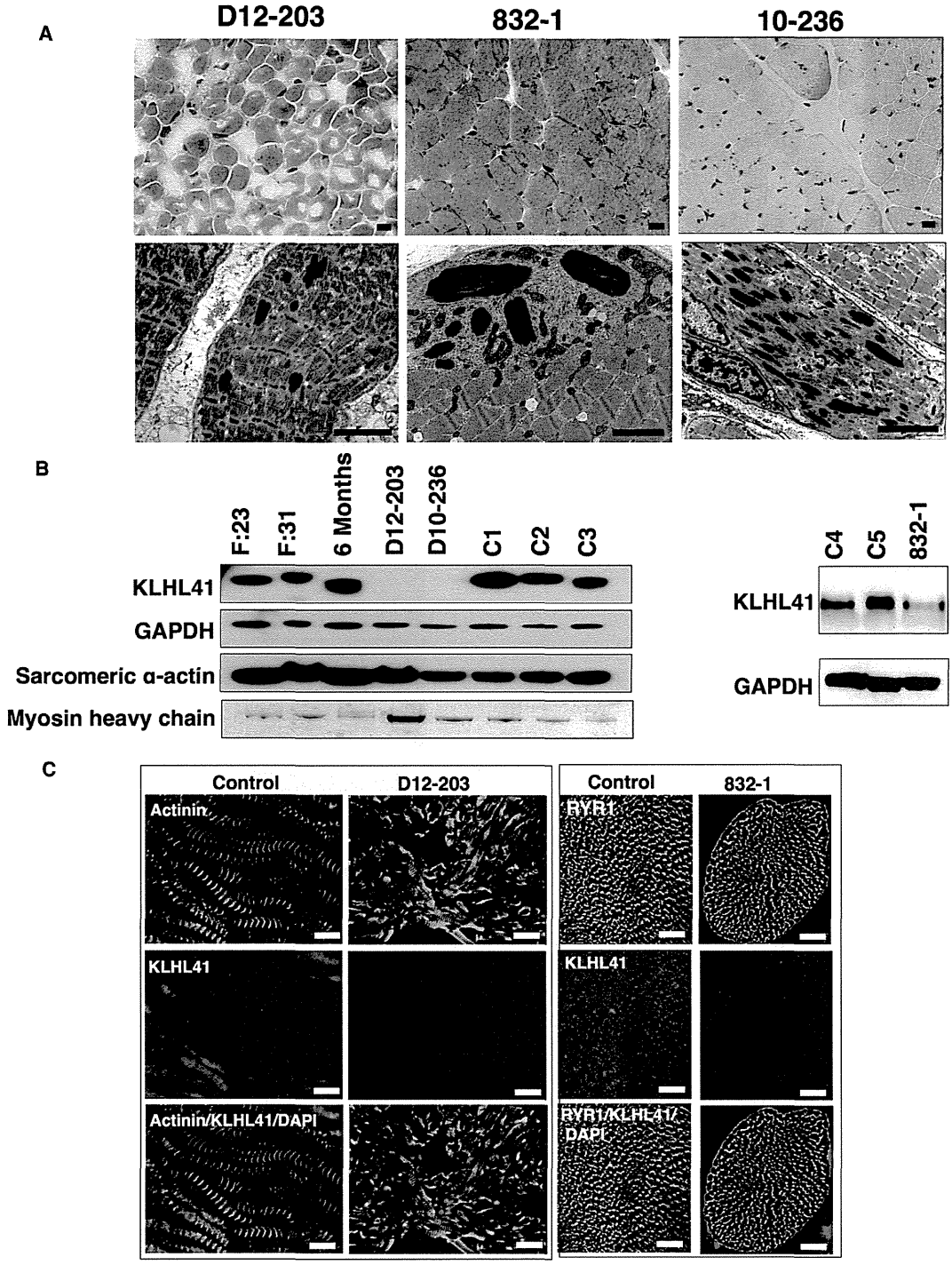

Figure 2. Muscle Pathology and Expression of KLHL41 Levels and Localization in Muscle of Affected Individuals

(A) Light microscopy of Gomori trichrome stained skeletal muscle from affected individuals with *KLHL41* mutations show cytoplasmic nemaline bodies (top panel). Electron microscopy of affected muscles reveals rods of variable frequency and size and severe myofibrillar disarray (bottom panels). (Scale bars represent 2 μm). Affected individuals' IDs are indicated at top.

(B) Immunoblotting analysis of KLHL41 levels in affected and unaffected muscles. A decrease in protein levels was observed in individuals with *KLHL41* mutations in comparison to normal control muscles. Immunoblotting with sarcomeric actin or Coomassie staining of myosin heavy chain showed no abnormal accumulation of sarcomeric proteins in affected muscles. Immunostaining for GAPDH was used for loading controls. Lanes: F:23, 23 week control fetus; F:30, 31 week control fetus; 6-month-old control baby, C1–C5 are normal age-matched control muscles.

(C) Immunofluorescence for KLHL41 in control and affected individual muscle biopsies showed highly reduced levels of KLHL41 in longitudinally oriented (left) or transverse sections (right) of skeletal muscles from affected individuals. Scale bars represent 50 μm.

Please cite this article in press as: Gupta et al., Identification of *KLHL41* Mutations Implicates BTB-Kelch-Mediated Ubiquitination as an Alternate Pathway to..., The American Journal of Human Genetics (2013), http://dx.doi.org/10.1016/j.ajhg.2013.10.020

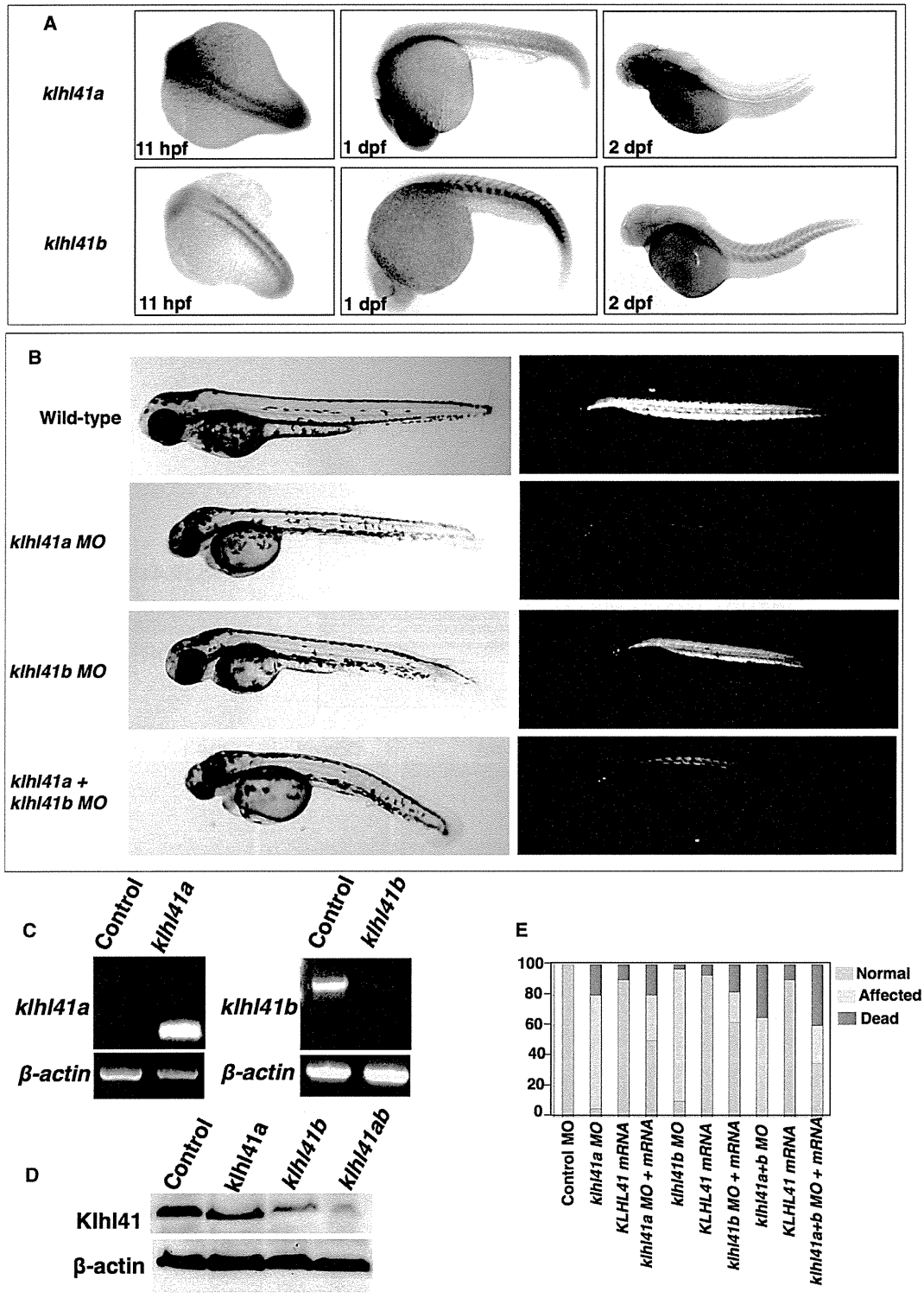

Figure 3. Characterization and Knockdown of Zebrafish Orthologs of *KLHL41*

(A) In situ hybridization of the zebrafish Klhl41 genes shows early expression during myogenesis in developing somites (11 hr after fertilization). *Klhl41a* is expressed in brain, eyes, and muscle at 1 dpf. Later in development expression is largely restricted to brain and heart (2 dpf), although low levels of expression in axial slow skeletal myofibers cannot be excluded due to limited sensitivity of the assay. *Klhl41b* expression is localized to skeletal muscle and heart at all developmental stages (1–2 dpf).

(B) Knockdown of Klhl41 genes in zebrafish using antisense morpholinos results in myopathic changes. Live microscopy of zebrafish embryos at 3 dpf reveals leaner and smaller bodies in comparison to wild-type (WT) fish. Under polarized microscopy, zebrafish embryos

(legend continued on next page)

previously.[24] Immunofluorescence with both antibodies resulted in similar staining patterns; however, due to lower background staining, the C-terminal antibody was used for further studies. Costaining with sarcomeric markers in longitudinal planes showed that KLHL41 staining predominated over the I-bands of the sarcomere and at perinuclear regions in human biopsies (Figure 2C) and murine cultured myofibers (Figure S4). Analysis of transverse sections of myofibers from control human biopsies revealed KLHL41 staining in a ring pattern around the myofibrils, generally colocalizing with ryanodine receptors (RYR1), which are a marker of the sarcoplasmic reticulum (Figure S5). Together, these observations suggest that KLHL41 localizes over (but not within) I bands, likely in association with the terminal cisternae of the sarcomplasmic reticulum (SR) and longitudinal vesicles of the SR present in the I-band area at the triadic regions (Figure S4). Colocalization studies with the ER marker protein disulfide isomerase (PDI) in myofibers and skeletal muscles further confirmed the localization of KLHL41 in SR-ER membranes (Figures S4). This overall localization pattern is most consistent with localization to the endoplasmic reticulum (ER) around myonuclei and to microdomains of the SR with ER characteristics.[25] Previous studies suggested that the closely related NM protein, KLHL40, localized at A-bands,[13] but double label immunofluorescence studies of both longitudinal and transverse sections here reveal that it appears colocalized with RYR1, around but not within the myofibrils in cultured myofibers and human skeletal muscles in a pattern overlapping, but not identical to, that of KLHL41 (Figures S4 and S5). These associations of proteins whose defects cause NM with the ER/SR contrasts with previously known NM proteins, all of which are sarcomeric thin filament components, with the exception of KBTBD13 whose localization is not well known.

In mouse tissues, immunoblotting detected KLHL41 in skeletal muscle and diaphragm (Figure S6). In cultured murine C2C12 cells, KLHL41 levels increased during differentiation to myotubes (Figure S6). Immunoblotting of affected skeletal muscle extracts revealed greatly reduced levels of KLHL41 in individuals with *KLHL41* mutations (Figure 2B) and immunofluorescence microscopy of affected individuals' skeletal muscles also showed that KLHL41 levels were greatly reduced in their myofibers (Figure 2C).

Cell culture studies have shown that KLHL41 interacts with nebulin, N-RAP (Nebulin-related anchoring protein), and actin in skeletal muscle and promotes the assembly of myofibrils.[26] KLHL41 regulates skeletal muscle differentiation as overexpression or knockdown inhibited C2C12 myoblast differentiation.[27] Knockdown of *Klhl41* in cultured cardiomyocytes resulted in sarcomeric disorganization with thickening of Z-lines as seen in NM.[28] However, the exact functions of KLHL41 in disease pathology are unknown. Recent studies have identified mutations in two other closely related family members *KBTBD13* and *KLHL40* as causes of NM suggesting the crucial requirement for several Kelch family proteins in skeletal muscle function.[12,13] To investigate the functional role of KLHL41 in vertebrate skeletal muscle development, we employed zebrafish as a model system. Zebrafish have two duplicated orthologs (*klhl41a* and *klhl41b*) that share ~80% similarity with *KLHL41*. Zebrafish whole-mount in situ hybridization was performed to study the spatio-temporal expression of these genes during zebrafish development as described previously.[29] Specifically, RNA probes specific for each Klhl41 gene were generated by amplification of the 3′ UTRs from a cDNA library of 2 day postfertilization (dpf) zebrafish embryos, followed by in vitro transcription to generate digoxigenin-labeled antisense transcripts (primer sequences are provided in Table S1). Whole-mount in situ hybridization showed ubiquitous expression of *klhl41a* during early development at 1 dpf, but by 2 dpf, *klhl41a* transcripts were virtually undetectable in the major axial skeletal muscles. In contract, *klhl41b* expression was predominantly seen in striated muscles, and strong expression in heart and skeletal muscles was observed throughout zebrafish development to at least 5 dpf (Figure 3A).

The effect of KLHL41 deficiency in zebrafish was studied by knocking down the Klhl41 genes with antisense morpholinos. Two independent morpholinos targeting an exon-intron spice site and translational start site were designed for both genes (morpholino sequences are provided in Table S2). As initial experiments with both morpholinos for each transcript resulted in similar phenotypes, we performed the remainder of our studies with the splice-site morpholinos (7 ng). *klhl41a* morphants exhibited leaner bodies, smaller eyes, and pericardial edema as seen in other myopathy models (n = 65–110) (Figure 3B).[30,31] Examination of 3 dpf morphants with polarized light showed reduced birefringence in axial skeletal muscles suggesting disorganized skeletal muscle structure (Figure 3B; Figure S7). Knockdown of *klhl41b*

exhibit a reduction in birefringence in morphant fish, quantified in ImageJ as described (WT controls: 100% ± 5.9% *klhl41a*: 23% ± 3.0%; *klhl41b*: 31% ± 8.2%; *klhl41ab*: 16% ± 4.2%). Double knockdown fish show a more severe skeletal muscle phenotype than single morphants.

(C) RT-PCR analysis showed knockdown of normal transcripts in the morphant fish.

(D) Immunoblot analysis showed reduction in Klhl41 levels in *klhl41a*, *klhl41b*, and *klhl41ab* fish. Klhl41 antibody recognizes both klhl41a and klhl41b and therefore show immunoreactibility to the other gene in the single morphants that is highly reduced in double morphants.

(E) Overexpression of human *KLHL41* mRNA restores the skeletal muscle phenotypes of *klhl41a/b* single and double morphants suggesting morpholino specificity. The mRNA concentration used to rescue were as follows: *klhl41a* (50 pg), *klhl41b* (75 pg), *klhl41a+b* (60 pg of each)

Please cite this article in press as: Gupta et al., Identification of *KLHL41* Mutations Implicates BTB-Kelch-Mediated Ubiquitination as an Alternate Pathway to..., The American Journal of Human Genetics (2013), http://dx.doi.org/10.1016/j.ajhg.2013.10.020

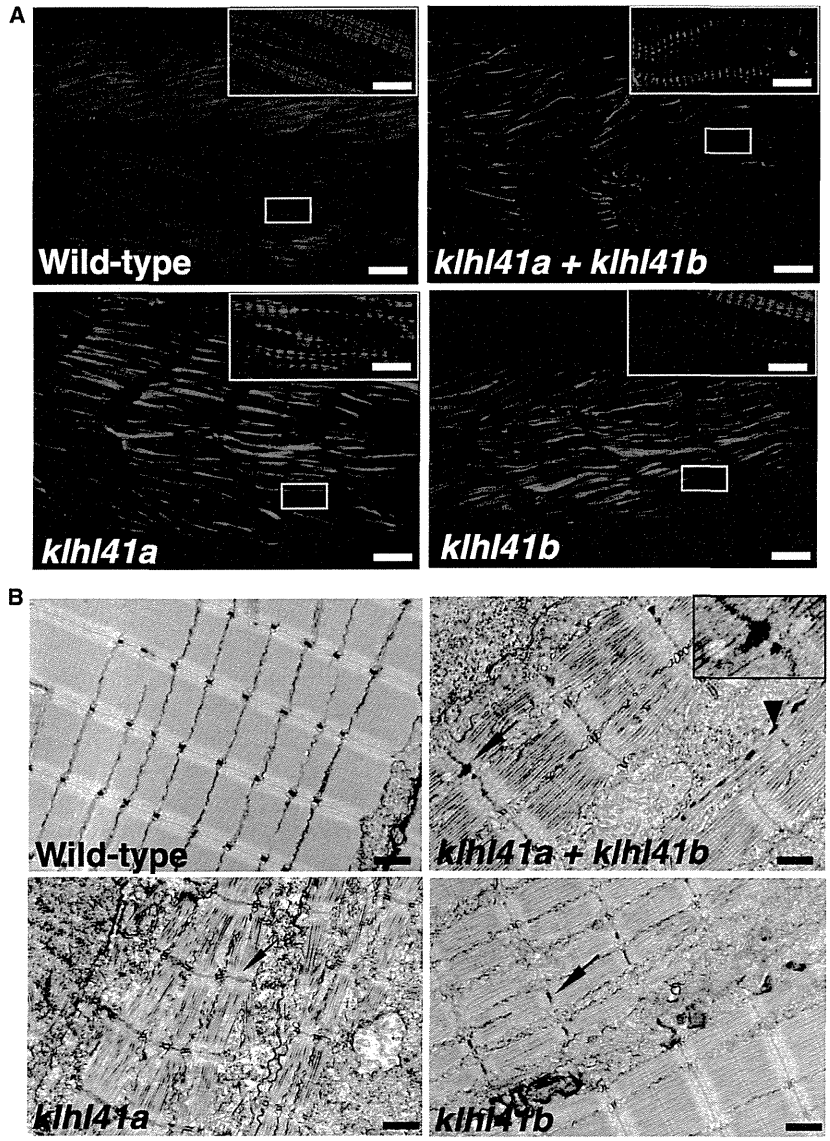

Figure 4. Loss of *klhl41* Function in Zebrafish Recapitulates the Disease Pathology of Human Nemaline Myopathies
(A) Whole-mount staining of 3 dpf zebrafish embryos with phalloidin showed extensive myofibrillar disarray of myofibers in *klhl41* morphant fish (scale bar represents 2 μm). Three dpf embryos fixed in 4% paraformaldehyde were incubated with phalloidin (Invitrogen, A12380, 1:40) overnight at 4°C. Skeletal muscles of klhl41-deficient embryos were smaller and exhibited an overall reduction of myofibrillar organization (inset, high magnification).
(B) Electron microscopy of klhl41-deficient skeletal muscle revealed thickened Z-lines in *klhl41a* or *klhl41b* morphants. In addition, skeletal muscle of double knockdown fish contained electron dense bodies, reminiscent of nascent nemaline rods (arrowhead, nemaline bodies like structures; arrow, thickened Z-lines) (scale bar represents 1 μm).

resulted in reduced birefringence without any other significant abnormalities (n = 82–132). Targeting both *klhl41a* and *klhl41b* (7 ng each) resulted in curved bodies with a 30% reduction in size along with small eyes and pericardial edema (n = 89–103), compared to fish injected with control morpholino (14ng). *klhl41a* morphant fish die by 3 dpf while *klhl41b* morphants typically did not survive past 5 dpf. Knockdown of both genes was lethal by 3 dpf. Double knockdown fish exhibited severely disorganized muscle (measured by reduced birefringence) compared to controls and either of the single knockdowns. RT-PCR and immunoblotting confirmed the knockdown of *klhl41a* and *klhl41b* transcripts and a reduction in protein levels (Figures 3C and 3D). Overexpression of human *KLHL41* mRNA in the double morphants resulted in a significant increase in the number of surviving fish with normal birefringence suggesting the specificity of morpholino injections and demonstrating the ability of this single evolutionary ortholog to complement both zebrafish genes (Figure 3E). Behavioral characterization of 3 dpf morphant fish, knocked down for either or both Klhl41 genes, using the touch-evoked response assay showed significantly diminished motility in comparison to control fish (WT fish: 5.74 ± 0.98 cm/0.1 s; *klhl41a*: 1.32 ± 0.61 cm/0.1 s; *klhl41b*: 2.00 ± 0.49 cm/0.1 s; *klhl41ab*: 0.73 ± 0.39 cm/0.1 s), suggesting a significant degree of overall muscle weakness (Movies S1, S2, S3, and S4).[32] To visualize abnormalities in sarcomeric architecture, whole-mount staining of morphant fish and control zebrafish embryos was performed with phalloidin to stain the actin-thin filaments. Although well-organized myofibrillar striations (i.e., sarcomeres) were observed, the myofibrils in *klhl41* morphants tended to be thinner and were highly disorganized relative to control fish (Figure 4A). The myofibrilar disorganization in *klhl41* morphants was also evident by evaluation of ultrathin toluidine blue sections of control and morphant fish (Figure S7). The main diagnostic feature of NM is the presence of nemaline rods with or without Z-line streaming in skeletal muscle. Ultrastructural examination of zebrafish skeletal muscle by electron microscopy showed Z-line thickening in both *klhl41a* and *klhl41b* morphant fish (Figure 4B). Knockdown of both *klhla* and *klhl41b* resulted in the presence of numerous electron-dense structures, reminiscent of small or nascent nemaline bodies, in addition to Z-line thickening (Figure 4B). Given the differences in temporal expression of *klhl41a* (early embryogenesis) and *klhl41b*

(maintained later in development), and the high degree of structural and functional conservation (both are rescued by the single human transcript), it is likely that increased severity of *klhl41a* morphants is due to this being the predominant embryonic isoform at the early stages targeted by morpholino injections.

Extensive skeletal muscle disorganization associated with sarcomeric abnormalities in morphant fish points toward a function of KLHL41 in skeletal muscle development and maintenance. Mutations affecting the closely related BTB-Kelch family member KLHL40 have recently also been reported to cause nemaline myopathy.[13] While *KLHL40* mutations resulted in a severe clinical presentation in most of the affected individuals, KLHL41 abnormalities are associated with a spectrum of phenotypes from severe with neonatal death, to survival into late childhood. However, no significant differences were seen in skeletal muscle pathology. KLHL40 contains a putative nuclear localization sequence (NLS) and is expressed throughout muscle differentiation, whereas KLHL41 lacks NLS and is expressed in late differentiation (Figure S8).[13] KLHL41 and many other BTB domain-containing Kelch family members are known to interact with Cul3 ubiquitin ligase to form functional ubiquitination complexes with proteins targeted for degradation.[21,33] KLHL41, which has been shown to interact with nebulin,[34] is now the third BTB-Kelch family member to be identified as a cause of NM when mutated. We hypothesize that improper surveillance and degradation of aberrant thin-filament proteins might explain the convergent pathological and clinical phenotypes associated with mutations of thin filament and BTB-Kelch family member genes in NM.

Supplemental Data

Supplemental Data include eight figures, two tables, and four movies and can be found with this article online at http://www.cell.com/AJHG/home.

Acknowledgments

We are grateful to the many NM affected individuals and their families, and to their treating physicians, for their participation in this research. Whole-exome sequencing was made possible through the generous support and assistance of David Margulies and the entire staff of The Gene Partnership Project at Boston Children's Hospital. We would like to thank Pankaj Agrawal and Wen-Hann Tan for many helpful discussions during the course of this work. We are thankful to Louise Trakimas of the electron microscope facility at Harvard Medical School for excellent help with zebrafish histology, and the Genotyping and Sequencing Core Facilities at KFSHRC for their technical help. V.A.G. is supported by K01 AR062601 from the National Institute of Arthritis and Musculoskeletal and Skin Diseases of National Institute of Health. This work was also supported by the Muscular Dystrophy Association of USA (MDA201302), National Institutes of Health grant from the National Institute of Arthritis and Musculoskeletal and Skin Diseases R01 AR044345, the AUism Charitable Foundation, and A Foundation Building Strength (to A.H.B.); National Health and Medical Research Council of Australia Early Career Researcher Fellowship #1035955 (to G.R.); Research Fellowship APP1002147 and Project Grant APP1022707(to N.G.L.); the Association Française contre les Myopathies (#15734), Dubai-Harvard Foundation for Medical Research Collaborative Research Grant (to F.S.A.); a UWA Collaborative Research Award (G.R.); and the Great Ormond Street Hospital Children's Charity (to F.M.). E.J.T. and K.S.Y. are supported by University of Western Australia Postgraduate Awards. DNA sequencing was performed by the Boston Children's Hospital Genomics Program Molecular Genetics Core, and confocal microscopy was performed at Boston Children's Hospital Intellectual and Developmental Disability Research Center Imaging Core, both supported by National Institutes of Health grant P30 HD18655. The funders had no role in study design, data collection and analysis, decision to publish, or preparation of the manuscript.

Received: August 9, 2013
Revised: October 15, 2013
Accepted: October 22, 2013
Published: November 21, 2013

Web Resources

The URLs for data presented herein are as follows:

1000 Genomes, http://browser.1000genomes.org
dbSNP, http://www.ncbi.nlm.nih.gov/projects/SNP/
NHLBI Exome Sequencing Project (ESP) Exome Variant Server, http://evs.gs.washington.edu/EVS/
Online Mendelian Inheritance in Man (OMIM), http://www.omim.org/
Picard, http://picard.sourceforge.net/
Pymol, http://www.pymol.org

References

1. Wallgren-Pettersson, C., Sewry, C.A., Nowak, K.J., and Laing, N.G. (2011). Nemaline myopathies. Semin. Pediatr. Neurol. *18*, 230–238.
2. Ryan, M.M., Schnell, C., Strickland, C.D., Shield, L.K., Morgan, G., Iannaccone, S.T., Laing, N.G., Beggs, A.H., and North, K.N. (2001). Nemaline myopathy: a clinical study of 143 cases. Ann. Neurol. *50*, 312–320.
3. Wallgren-Pettersson, C. (2002). Nemaline and myotubular myopathies. Semin. Pediatr. Neurol. *9*, 132–144.
4. Sewry, C.A. (2008). Pathological defects in congenital myopathies. J. Muscle Res. Cell Motil. *29*, 231–238.
5. Hutchinson, D.O., Charlton, A., Laing, N.G., Ilkovski, B., and North, K.N. (2006). Autosomal dominant nemaline myopathy with intranuclear rods due to mutation of the skeletal muscle ACTA1 gene: clinical and pathological variability within a kindred. Neuromuscul. Disord. *16*, 113–121.
6. Pelin, K., Hilpelä, P., Donner, K., Sewry, C., Akkari, P.A., Wilton, S.D., Wattanasirichaigoon, D., Bang, M.L., Centner, T., Hanefeld, F., et al. (1999). Mutations in the nebulin gene associated with autosomal recessive nemaline myopathy. Proc. Natl. Acad. Sci. USA *96*, 2305–2310.
7. Nowak, K.J., Wattanasirichaigoon, D., Goebel, H.H., Wilce, M., Pelin, K., Donner, K., Jacob, R.L., Hübner, C., Oexle, K., Anderson, J.R., et al. (1999). Mutations in the skeletal muscle

alpha-actin gene in patients with actin myopathy and nemaline myopathy. Nat. Genet. *23*, 208–212.

8. Laing, N.G., Wilton, S.D., Akkari, P.A., Dorosz, S., Boundy, K., Kneebone, C., Blumbergs, P., White, S., Watkins, H., Love, D.R., et al. (1995). A mutation in the alpha tropomyosin gene TPM3 associated with autosomal dominant nemaline myopathy. Nat. Genet. *9*, 75–79.
9. Tajsharghi, H., Ohlsson, M., Lindberg, C., and Oldfors, A. (2007). Congenital myopathy with nemaline rods and cap structures caused by a mutation in the beta-tropomyosin gene (TPM2). Arch. Neurol. *64*, 1334–1338.
10. Agrawal, P.B., Greenleaf, R.S., Tomczak, K.K., Lehtokari, V.L., Wallgren-Pettersson, C., Wallefeld, W., Laing, N.G., Darras, B.T., Maciver, S.K., Dormitzer, P.R., and Beggs, A.H. (2007). Nemaline myopathy with minicores caused by mutation of the CFL2 gene encoding the skeletal muscle actin-binding protein, cofilin-2. Am. J. Hum. Genet. *80*, 162–167.
11. Johnston, J.J., Kelley, R.I., Crawford, T.O., Morton, D.H., Agarwala, R., Koch, T., Schäffer, A.A., Francomano, C.A., and Biesecker, L.G. (2000). A novel nemaline myopathy in the Amish caused by a mutation in troponin T1. Am. J. Hum. Genet. *67*, 814–821.
12. Sambuughin, N., Yau, K.S., Olivé, M., Duff, R.M., Bayarsaikhan, M., Lu, S., Gonzalez-Mera, L., Sivadorai, P., Nowak, K.J., Ravenscroft, G., et al. (2010). Dominant mutations in KBTBD13, a member of the BTB/Kelch family, cause nemaline myopathy with cores. Am. J. Hum. Genet. *87*, 842–847.
13. Ravenscroft, G., Miyatake, S., Lehtokari, V.L., Todd, E.J., Vornanen, P., Yau, K.S., Hayashi, Y.K., Miyake, N., Tsurusaki, Y., Doi, H., et al. (2013). Mutations in KLHL40 are a frequent cause of severe autosomal-recessive nemaline myopathy. Am. J. Hum. Genet. *93*, 6–18.
14. Li, H., and Durbin, R. (2009). Fast and accurate short read alignment with Burrows-Wheeler transform. Bioinformatics *25*, 1754–1760.
15. Wang, K., Li, M., and Hakonarson, H. (2010). ANNOVAR: functional annotation of genetic variants from high-throughput sequencing data. Nucleic Acids Res. *38*, e164.
16. Alkuraya, F.S. (2012). Discovery of rare homozygous mutations from studies of consanguineous pedigrees. Curr Protoc Hum Genet. *Chapter 6*, Unit 6, 12.
17. Adams, J., Kelso, R., and Cooley, L. (2000). The kelch repeat superfamily of proteins: propellers of cell function. Trends Cell Biol. *10*, 17–24.
18. Dhanoa, B.S., Cogliati, T., Satish, A.G., Bruford, E.A., and Friedman, J.S. (2013). Update on the Kelch-like (KLHL) gene family. Hum. Genomics *7*, 13.
19. du Puy, L., Beqqali, A., van Tol, H.T., Monshouwer-Kloots, J., Passier, R., Haagsman, H.P., and Roelen, B.A. (2012). Sarcosin (Krp1) in skeletal muscle differentiation: gene expression profiling and knockdown experiments. Int. J. Dev. Biol. *56*, 301–309.
20. Gray, C.H., McGarry, L.C., Spence, H.J., Riboldi-Tunnicliffe, A., and Ozanne, B.W. (2009). Novel beta-propeller of the BTB-Kelch protein Krp1 provides a binding site for Lasp-1 that is necessary for pseudopodial extension. J. Biol. Chem. *284*, 30498–30507.
21. Canning, P., Cooper, C.D., Krojer, T., Murray, J.W., Pike, A.C., Chaikuad, A., Keates, T., Thangaratnarajah, C., Hojzan, V., Marsden, B.D., et al. (2013). Structural basis for Cul3 protein assembly with the BTB-Kelch family of E3 ubiquitin ligases. J. Biol. Chem. *288*, 7803–7814.
22. Spence, H.J., Johnston, I., Ewart, K., Buchanan, S.J., Fitzgerald, U., and Ozanne, B.W. (2000). Krp1, a novel kelch related protein that is involved in pseudopod elongation in transformed cells. Oncogene *19*, 1266–1276.
23. Guerois, R., Nielsen, J.E., and Serrano, L. (2002). Predicting changes in the stability of proteins and protein complexes: a study of more than 1000 mutations. J. Mol. Biol. *320*, 369–387.
24. Lawlor, M.W., Alexander, M.S., Viola, M.G., Meng, H., Joubert, R., Gupta, V., Motohashi, N., Manfready, R.A., Hsu, C.P., Huang, P., et al. (2012). Myotubularin-deficient myoblasts display increased apoptosis, delayed proliferation, and poor cell engraftment. Am. J. Pathol. *181*, 961–968.
25. Kaisto, T., and Metsikkö, K. (2003). Distribution of the endoplasmic reticulum and its relationship with the sarcoplasmic reticulum in skeletal myofibers. Exp. Cell Res. *289*, 47–57.
26. Lu, S., Carroll, S.L., Herrera, A.H., Ozanne, B., and Horowits, R. (2003). New N-RAP-binding partners alpha-actinin, filamin and Krp1 detected by yeast two-hybrid screening: implications for myofibril assembly. J. Cell Sci. *116*, 2169–2178.
27. Paxton, C.W., Cosgrove, R.A., Drozd, A.C., Wiggins, E.L., Woodhouse, S., Watson, R.A., Spence, H.J., Ozanne, B.W., and Pell, J.M. (2011). BTB-Kelch protein Krp1 regulates proliferation and differentiation of myoblasts. Am. J. Physiol. Cell Physiol. *300*, C1345–C1355.
28. Greenberg, C.C., Connelly, P.S., Daniels, M.P., and Horowits, R. (2008). Krp1 (Sarcosin) promotes lateral fusion of myofibril assembly intermediates in cultured mouse cardiomyocytes. Exp. Cell Res. *314*, 1177–1191.
29. Gupta, V., Discenza, M., Guyon, J.R., Kunkel, L.M., and Beggs, A.H. (2012). α-Actinin-2 deficiency results in sarcomeric defects in zebrafish that cannot be rescued by α-actinin-3 revealing functional differences between sarcomeric isoforms. FASEB J. *26*, 1892–1908.
30. Dowling, J.J., Vreede, A.P., Low, S.E., Gibbs, E.M., Kuwada, J.Y., Bonnemann, C.G., and Feldman, E.L. (2009). Loss of myotubularin function results in T-tubule disorganization in zebrafish and human myotubular myopathy. PLoS Genet. *5*, e1000372.
31. Gupta, V.A., Kawahara, G., Myers, J.A., Chen, A.T., Hall, T.E., Manzini, M.C., Currie, P.D., Zhou, Y., Zon, L.I., Kunkel, L.M., and Beggs, A.H. (2012). A splice site mutation in laminin-α2 results in a severe muscular dystrophy and growth abnormalities in zebrafish. PLoS ONE *7*, e43794.
32. Smith, L.S., Beggs, A.H., and Gupta, V.A. (2013). Analysis of skeletal muscle defects in larval zebrafish by birefringence and touch-evoke escape response assays. J. Vis. Exp. *82*, e50925. http://dx.doi.org/10.3791/50925.
33. Zhang, D.D., Lo, S.C., Sun, Z., Habib, G.M., Lieberman, M.W., and Hannink, M. (2005). Ubiquitination of Keap1, a BTB-Kelch substrate adaptor protein for Cul3, targets Keap1 for degradation by a proteasome-independent pathway. J. Biol. Chem. *280*, 30091–30099.
34. Spence, H.J., McGarry, L., Chew, C.S., Carragher, N.O., Scott-Carragher, L.A., Yuan, Z., Croft, D.R., Olson, M.F., Frame, M., and Ozanne, B.W. (2006). AP-1 differentially expressed proteins Krp1 and fibronectin cooperatively enhance Rho-ROCK-independent mesenchymal invasion by altering the function, localization, and activity of nondifferentially expressed proteins. Mol. Cell. Biol. *26*, 1480–1495.

ARTICLE IN PRESS

Available online at www.sciencedirect.com

SciVerse ScienceDirect

Neuromuscular Disorders xxx (2013) xxx–xxx

www.elsevier.com/locate/nmd

Case report

Fatal hepatic hemorrhage by peliosis hepatis in X-linked myotubular myopathy: A case report

T. Motoki [a,*], M. Fukuda [d], T. Nakano [a], S. Matsukage [b], A. Fukui [c], S. Akiyoshi [e], Y.K. Hayashi [f,g], E. Ishii [d], I. Nishino [f,g]

[a] *Department of Pediatrics, Uwajima City Hospital, Uwajima, Ehime, Japan*
[b] *Pathology, Uwajima City Hospital, Uwajima, Ehime, Japan*
[c] *Radiology, Uwajima City Hospital, Uwajima, Ehime, Japan*
[d] *Department of Pediatrics, Ehime University Graduate School of Medicine, Toon, Ehime, Japan*
[e] *Department of Neonatology, Ehime Prefectural Central Hospital, Matsuyama, Ehime, Japan*
[f] *Department of Neuromuscular Research, National Institute of Neuroscience, National Center of Neurology and Psychiatry (NCNP), Tokyo, Japan*
[g] *Department of Clinical Development, Translational Medical Center, NCNP, Kodaira, Tokyo, Japan*

Received 31 October 2012; received in revised form 4 May 2013; accepted 11 June 2013

Abstract

We report a 5-year-old boy with X-linked myotubular myopathy complicated by peliosis hepatis. At birth, he was affected with marked generalized muscle hypotonia and weakness, which required permanent ventilatory support, and was bedridden for life. He died of acute fatal hepatic hemorrhage after using a mechanical in-exsufflator. Peliosis hepatis, defined as multiple, variable-sized, cystic blood-filled spaces through the liver parenchyma, was confirmed by autopsy. To avoid fatal hepatic hemorrhage by peliosis hepatis, routine hepatic function tests and abdominal imaging tests should be performed for patients with X-linked myotubular myopathy, especially at the time of using artificial respiration.

Keywords: X-linked myotubular myopathy; Hepatic hemorrhage; Peliosis hepatis; Mechanical in-exsufflator

1. Introduction

X-linked myotubular myopathy (XLMTM) is one of the most serious types of centronuclear ("myotubular") myopathies, which is pathologically characterized by a high proportion of small myofibers with centrally placed nuclei [1]. With recent advances in molecular analysis, centronuclear myopathy has been classified into three genetic subtypes. XLMTM is a severe form of centronuclear myopathy presenting with symptoms from birth, including respiratory failure, ophthalmoplegia, and muscle weakness [2]. XLMTM is caused by genetic aberration of the *MTM1* gene on chromosome Xq28 [3]. *MTM1* encodes myotubularin, a dual-specificity 3-phosphoinositide phosphatase, which plays an important role in the regulation of signaling pathways involved in muscle growth and differentiation [3].

Although XLMTM is considered to be a fatal disorder within the first year of life, it has been recently shown that more than half of XLMTM patients achieve prolonged survival, and most of the long-term survivors suffer from several complications in several organ systems [4]. Among them, peliosis hepatis is a rare condition that can affect children and cause fatal hepatic hemorrhage. A few reports have suggested that XLMTM patients might be at risk for development of peliosis hepatis [4–7]. We report a 5-year-old patient with XLMTM who suffered

* Corresponding author. Address: Department of Pediatrics, Uwajima City Hospital, 1-1 Goten-cho, Uwajima, Ehime 798-8510, Japan. Tel.: +81 895 25 1111; fax: +81 895 25 5334.
E-mail address: tmotoki@m.ehime-u.ac.jp (T. Motoki).

0960-8966/$ - see front matter © 2013 Elsevier B.V. All rights reserved.
http://dx.doi.org/10.1016/j.nmd.2013.06.008

Please cite this article in press as: Motoki T et al., Fatal hepatic hemorrhage by peliosis hepatis in X-linked myotubular myopathy: A case report, Neuromuscul Disord (2013), http://dx.doi.org/10.1016/j.nmd.2013.06.008

from fatal peliosis hepatis. In addition, the clinical features and prevention approach of fatal hepatic hemorrhage in XLMTM are also discussed.

2. Case report

A full-term male was born at 39 weeks of gestational age by normal spontaneous vaginal delivery and weighed 2728 g. The Apgar score was 5 at 1 min and 7 at 5 min. There was no abnormal antenatal symptom (e.g. polyhydramnios, reduced fetal movements, and thinning of the ribs). And neither family history of genetic disorders nor medical problem during perinatal period was observed. At birth, however, marked generalized muscle hypotonia and weakness, which required ventilatory support, appeared in the patient. On physical examination, facial muscle weakness and a high-arched palate were detected, and extraocular muscle involvement was not detected. The hypotonia did not improve with conventional management. The karyotype of peripheral blood was normal. A muscle biopsy from the biceps branch was performed under the possible diagnosis of neuromuscular disease. All muscle fibers were small and round (Fig. 1a), and a peripheral halo was observed in most fibers (Fig. 1b), compatible with the diagnosis of myotubular myopathy. Type 1 fiber predominance was remarkable (90%) (Fig. 1c). Genetic analysis of XLMTM revealed a splice-acceptor-site mutation of *MTM1* in intron 6 (c.445-1G>A), resulting in skipping of exon 7 at the cDNA level (Fig. 1d) [8]. The patient received respiratory support using non-invasive positive pressure ventilation, and underwent a tracheotomy at 8 months of age because of frequent asphyxia caused by aspiration.

At 5 years old, he was admitted to the Uwajima City Hospital for treatment of massive pneumonia and atelectasis in the left lung. Laboratory studies on admission showed that hemoglobin was 14.6 g/dL, white blood cell count was 11,400/μL, platelet count was 338,000/μL, aspartate aminotransferase was 69 IU/L, alkaline phosphatase was 73 IU/L, and C-reactive protein was 0.46 mg/dL. Bacterial blood and sputum cultures showed negative results. Fibrinolytic activity test on four days after admission remained within normal limits (prothorombin time was 11.9 s, fibrin degradation products was 8.6 μg/ml and D-dimer was 0.8 μg/ml). The patient gradually improved with a course of antibiotics (cefotaxime sodium) and lung physical therapy. Nine days after admission, a mechanically assisted coughing system was used as a mechanical in-exsufflator (MI-E) because of difficulty of sputum expectoration. The next day, he suffered from abrupt tachycardia and cyanosis. He had a peripheral coldness and his abdomen was gradually distended, especially the right costal margin, because of hepatic enlargement. Laboratory studies

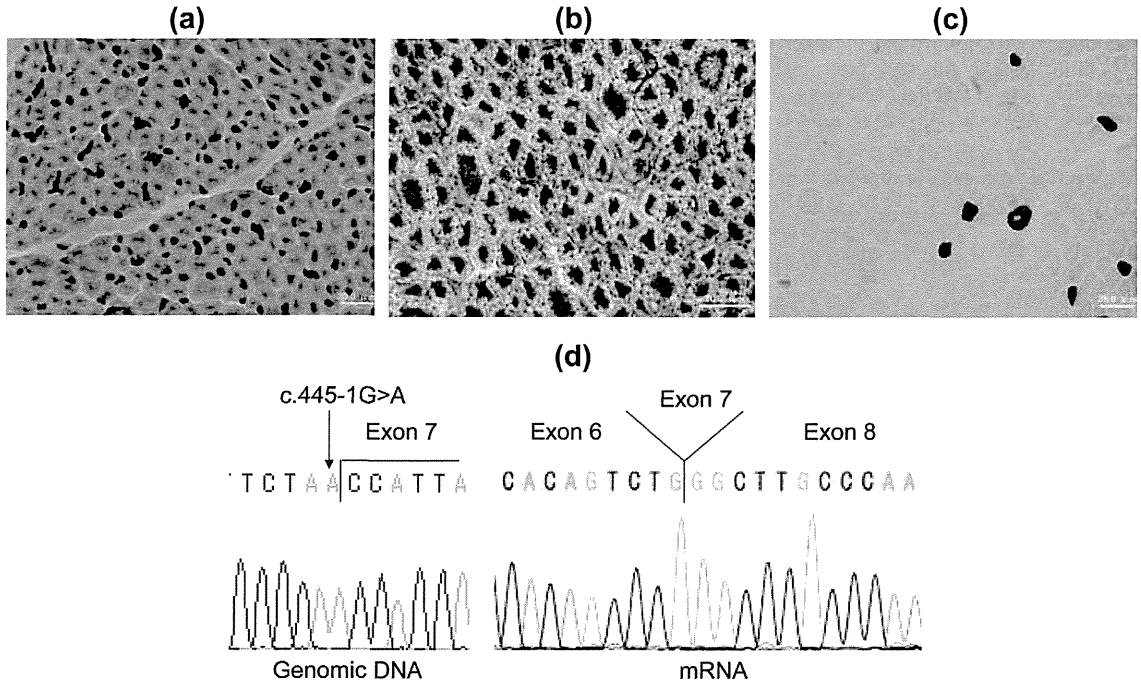

Fig. 1. Histological findings of muscle biopsy and genetic analysis. (a) Hematoxylin and eosin (H & E) staining shows that all muscle fibers are small and round. Marked perimysial fibrosis and scattered pyknotic nuclear clumps can be seen. Muscle fibers with central nuclei comprise 40% of the biopsy specimen. (b) As shown by nicotinamide adenine dinucleotide tetrazolium reductase staining, the intermyofibrillar network is markedly disorganized with peripheral halo features seen in most fibers. (c) On ATPase, types 1, 2A–C comprise 90%, 8%, 2%, and 0%, respectively. Type 2 fiber atrophy can be seen. (d) *MTM1* analysis revealed a splice-acceptor-site mutation in intron 6 (c.445-1G>A) at the genomic DNA level and skipping of exon 7 at the cDNA level.

Please cite this article in press as: Motoki T et al., Fatal hepatic hemorrhage by peliosis hepatis in X-linked myotubular myopathy: A case report, Neuromuscul Disord (2013), http://dx.doi.org/10.1016/j.nmd.2013.06.008

showed that the hemoglobin level and platelet count were decreased to 6.4 g/dL and 82,000/μL, respectively. An abdominal computed tomography (CT) scan showed hepatomegaly with a heterogeneous low density area expanding from the medial segment to the right lobe of the liver, and the leakage of contrast material into parenchyma during the arterial phase, suggesting the diagnosis of liver hemorrhage (Fig. 2a). There was little intraperitoneal bleeding. With rapid transfusion of red cells, a hepatic angiogram was performed via the common hepatic artery. Because active bleeding was observed within liver parenchyma (Fig. 2b), obstructing material (Gelpart® Molecular Devices, Nippon Kayaku Co. Ltd., Tokyo, Japan) was injected into the anterior and posterior branches of the hepatic artery to control active bleeding. Despite these treatments, hemoglobin levels gradually decreased from 11.1 to 3.8 g/dL 8 h after the obstruction therapy. The abdomen was further distended and pitting edema appeared in the lower body. Repeated abdominal CT showed massive intraperitoneal bleeding compared with that of the previous day, and a narrowed inferior vena cava caused by hepatic enlargement was detected. He died 4 days after the onset of acute hepatic hemorrhage. The autopsy indicated

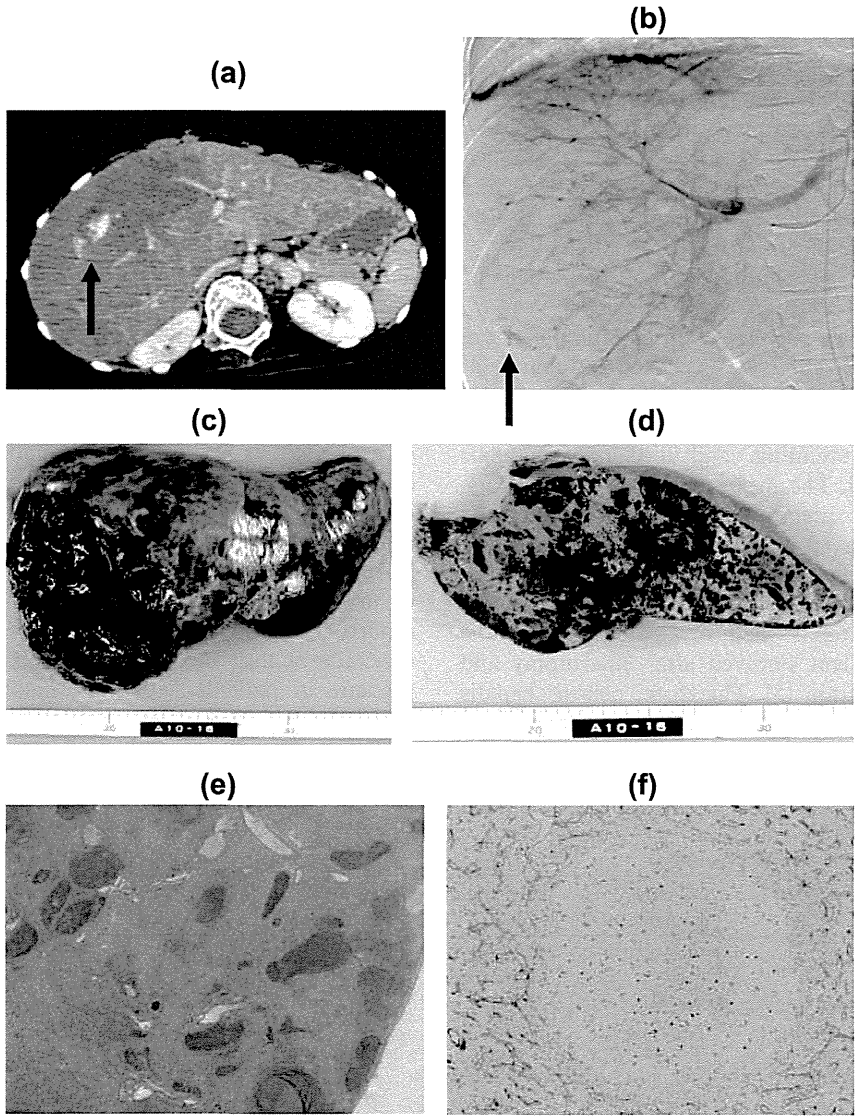

Fig. 2. Radiological and pathological findings of periosis hepatis. (a) Contrast abdominal CT shows hepatomegaly and a heterogeneous low density area extending from the medial segment to the right lobe of the liver. Contrast dye had leaked into the parenchyma (arrow) during the arterial phase. (b) A hepatic angiogram shows a number of retained contrast agents and some active bleeding (arrow) within liver parenchyma. (c and d) Autopsy findings show expansive intraperitoneal bleeding caused by rupture at the right hepatic capsule, and multiple variable-sized cystic blood-filled spaces were found in a section of the liver. (e) Multiple blood-filled spaces within the liver parenchyma can be seen (H & E). (f) Immunohistochemically, the inner surface of the blood-filled space is devoid of CD31-positive endothelial lining in contrast to the sinusoidal endothelia.

Please cite this article in press as: Motoki T et al., Fatal hepatic hemorrhage by peliosis hepatis in X-linked myotubular myopathy: A case report, Neuromuscul Disord (2013), http://dx.doi.org/10.1016/j.nmd.2013.06.008